

30 glitches in 18 radio pulsars

Hong-Yi Liu¹, Shi-Qi Zhou², Yu-Qi Zhang², Zhong-Wen Feng² and Xia Zhou²

¹ School of Applied Technology, XiHua University, Nanchong 637000, China

² Physics and Space Science College, China West Normal University, Nanchong 637009, China; sqzhou@nao.cas.cn

Received 2020 October 22; accepted 2020 December 25

Abstract Pulsar timing is a classic technology of detecting irregularities in pulsar rotation. We carried out this method for 18 young radio pulsars, with long-term timing observations obtained between 2007 and 2015 using the Parkes 64-m radio telescope. As a result, 30 glitches were identified, ranging from 0.75×10^{-9} to 8.6×10^{-6} in the relative glitch sizes $\Delta\nu/\nu$, where $\nu = 1/P$ is the pulse frequency. These glitches are composed of 26 new glitches and four published glitches with new exponential recoveries. All pulsars exhibit normal glitches, and six pulsars were observed to undergo a glitch event for the first time. We discuss the properties and implications for neutron-star physics of these glitches, and show that they are in agreement with previous work, except that the cumulative probability distributions of the mean waiting times for PSRs J0537–6910, J1341–6220 and J1740–3015 are not in consonance with the Poisson model.

Key words: methods: data analysis — stars: neutron — pulsars: general

1 INTRODUCTION

Pulsars are believed to be rotating magnetized neutron stars. Most of them are observed to regularly spin-down due to the loss of rotational energy. A pulsar glitch, which is characterized by an abrupt increase in spin frequency (ν), is a rare and bizarre phenomenon of irregularity in rotation. Such an event was first detected to occur in the Vela pulsar (Radhakrishnan & Manchester 1969; Reichley & Downs 1969). In the past 50 years, more than 545 glitches in 188 pulsars have been reported (for a complete list of these glitches, see the ATNF Pulsar Catalogue glitch table¹ or the Jodrell Bank Glitch Catalogue²). Most of these events are associated with young isolated normal pulsars. It is interesting that glitches are also detected in millisecond pulsars (Cognard & Backer 2004; McKee et al. 2016), the Hulse – Taylor binary pulsar (PSR B1913+16) (Weisberg et al. 2010), magnetars (Şaşmaz Muş et al. 2014) and accretion-powered binary pulsars (Serim et al. 2017).

The glitches have fractional sizes ($\Delta\nu/\nu$) ranging from 2.5×10^{-12} (McKee et al. 2016) to 1.37×10^{-3} (Serim et al. 2017). These sizes show a bimodal distribution with peaks at $\sim 10^{-6}$ and $\sim 10^{-9}$ (Lyne et al.

2000; Yuan et al. 2010; Yu et al. 2013). Larger glitches with an exponential recovery are more common in younger pulsars, whereas small glitches are more apt to change permanently for older pulsars (Zou et al. 2004). Glitch activity becomes evident in young pulsars with a characteristic age of $10^4 \sim 10^5$ yr (Wang et al. 2000; Espinoza et al. 2011). Smaller glitches would be less than expected because their identification is usually subjected to timing noise (Yu et al. 2013), which is another timing irregularity as a result of a continuous wandering of the pulsar spin rate (Lower et al. 2020). For almost all glitches, an abrupt increase in the spin frequency is accompanied by the sudden increase of spin-down rate (Palfreyman et al. 2018). Moreover, radiative changes are part of features in the glitch behaviors of magnetars (Dib & Kaspi 2014). Some glitches are linked to the variation of pulse emission (Kou et al. 2018; Palfreyman et al. 2018).

At present, the popular theory for pulsar glitches is angular momentum exchange between the faster rotating interior superfluid and the solid crust (Anderson & Itoh 1975; Alpar et al. 1981; Piekarewicz et al. 2014). From this theory, the superfluid can be regarded as a container of angular momentum. In some cases, angular momentum is transferred from the superfluid to crust, causing a spin-up of what we have seen in pulsars (Eya et al. 2017). Based on this model, Link et al. (1999) and Andersson et al. (2012) suggested that the ratio of neutron star components

¹ <https://www.atnf.csiro.au/people/pulsar/psrcat/glitchTbl.html>

² <http://www.jb.man.ac.uk/pulsar/glitches/gTable.html>

involved in period glitch can be estimated. On the other hand, Pizzochero et al. (2017) took a realistic approach to limit pulsar mass, in which the entire excess angular momentum is supposed to transfer to the crust in the maximum glitch. Pizzochero et al. (2017) also estimated the mass of all glitching pulsars that have displayed at least two large events. However, the discoveries of unusual glitch behaviors, such as slow glitch (Shabanova 2010; Zhou et al. 2019) and anti-glitch (Archibald et al. 2013; Ray et al. 2019), cast doubt on this standard pulsar glitch model. For the slow glitches, Shabanova (2009) suggested that this model cannot account for a slow exponential growth in spin frequency ν on timescales from several months to several years. Contrary to the model assumptions, anti-glitches imply that the interior superfluid is rotating more slowly than the solid crust (Şaşmaz Muş et al. 2014; Ray et al. 2019).

The properties and mechanism of pulsar glitches remain not fully understood. Therefore, there is great significance in increasing the sample of known spin-up events. For this paper, we searched for glitch events with timing observations from the Parkes 64-m radio telescope between 2007 and 2015. In Section 2, we describe the observations, and our method for determining glitch parameters. Section 3 features our results which focus on the glitch behaviors. Finally, we discuss and conclude our results in Section 4.

2 OBSERVATIONS AND ANALYSIS

Here, we analyzed the timing observations for 18 pulsars between 2007 and 2015, which are public for download from the Parkes pulsar data archive³ (Hobbs et al. 2011). Timing data on pulsars in this paper have been described in detail by Manchester et al. (2013). In short, our data were collected in the 20-cm band, having a central frequency of 1369 MHz and a bandwidth of 256 MHz. The multi-beam receiver and Parkes Digital Filter Bank backend systems have been used in the observations. Observing sessions have a typical interval of 2–4 weeks, with a sub-integration time of 30 s and integration times of 2–15 min.

The software packages PSRCRIVE (Hotan et al. 2004) and TEMPO2 (Hobbs et al. 2006) were applied to the off-line data reduction. The procedures include radio frequency interference (RFI) mitigation, polarization calibration, pulse profile folding, profile template creation, time-of-arrival (ToA) measurement by correlating the folded profile and the profile template, and timing residual determination. The ToAs were transformed to the Solar system barycenter (SSB) using the DE421 solar-system

ephemeris (Folkner et al. 2009). In actual data processing on pulsar glitches, we are more concerned with the rotational pulsar phase, which can be expressed by a Taylor expansion (Edwards et al. 2006)

$$\phi(t) = \phi(t_0) + \nu(t - t_0) + \frac{\dot{\nu}}{2}(t - t_0)^2 + \frac{\ddot{\nu}}{6}(t - t_0)^3, \quad (1)$$

where ν , $\dot{\nu}$ and $\ddot{\nu}$ represent the pulse frequency, its first derivative and second derivative, respectively.

A sudden discontinuity in the timing residuals provides clear evidence that a spin-up event occurred in a pulsar after fitting with parameters, such as the pulse frequency ν , its first derivative $\dot{\nu}$ and second derivative $\ddot{\nu}$. An additional pulse phase as a function of time is usually considered for describing a glitch as follows (Edwards et al. 2006; Yu et al. 2013)

$$\phi_g = \Delta\phi + \Delta\nu_p(t - t_g) + \frac{1}{2}\Delta\dot{\nu}_p(t - t_g)^2 + [1 - e^{-(t-t_g)/\tau_d}]\Delta\nu_d\tau_d, \quad (2)$$

where the first term on the right-hand side is an offset in pulse phase and t_g represents the glitch epoch. $\Delta\nu_p$ and $\Delta\dot{\nu}_p$ are the permanent changes in frequency and its first derivative relative to the extrapolated pre-glitch values. $\Delta\nu_d$ means the recovery amplitude of pulse frequency after time τ_d in an exponential decay process. Hence, the fractional glitch sizes can be expressed by the equation

$$\frac{\Delta\nu}{\nu} = \frac{\Delta\nu_p + \Delta\nu_d}{\nu}, \quad (3)$$

$$\frac{\Delta\dot{\nu}}{\dot{\nu}} = \frac{\Delta\dot{\nu}_p + \Delta\nu_d/\tau_d}{\dot{\nu}}.$$

Furthermore, the fraction of glitch recovery Q can be defined as $\Delta\nu_d/\Delta\nu$.

3 RESULT

Table 1 contains the basic parameters in the first seven columns with reference to literature: pulsar name, right ascension (J2000) and declination (J2000), epoch (MJD), pulsar period (P), period derivative (\dot{P}) and dispersion measure (DM). Since P and \dot{P} were provided, we calculated characteristic age $\tau_c = P/(2\dot{P})$ and surface dipole magnetic field $B_s = 3.2 \times 10^{19} \sqrt{P\dot{P}}$ in the next two columns. Moreover, our data spans are listed in the last column for each pulsar. Uncertainties refer to the corresponding last digits of the quoted results.

We referred to parameters listed in Table 1 and fitted Equation (1) to achieve phase-coherent timing solutions. In total, 30 glitches were identified because of phase discontinuities. Timing solutions (Table 2) were obtained from utilizing TEMPO2 to fit separately to pre- and post-glitch datasets. Table 2 gives the pulsar name and

³ <https://data.csiro.au/dap/public/atnf/pulsarSearch.zul>

Table 1 Parameters and Data Spans for 18 Glitching Pulsars

Pulsar Name (PSR)	RA (h m s)	DEC (d m s)	Epoch (MJD)	P (s)	\dot{P} (10^{-15})	DM (cm^{-3} pc)	Age (kyr)	B_s (10^{12} G)	Span (yr)
J0940–5428 ¹	09:40:58.22(4)	–54:28:40.6(3)	51091	0.0875	32.8683	134.55	42.2	1.72	6.7
J0954–5430 ¹	09:54:06.04(3)	–54:30:53.5(7)	51034	0.4728	43.912	201.57	171	4.61	4.0
J1016–5857 ²	10:16:21.16(1)	–58:57:12.1(1)	52717	0.1073	80.8340	394.2	21.0	2.98	6.7
J1019–5749 ³	10:19:52.14(4)	–57:49:05.9(5)	51371	0.1624	20.0770	1040	128	1.83	6.9
J1112–6103 ¹	11:12:14.81(4)	–61:03:31.1(6)	51055	0.0649	31.4590	599.1	32.7	1.45	4.8
J1248–6344 ³	12:48:46.36(5)	–63:44:09.6(5)	51451	0.1983	16.9180	433.0	186	1.85	6.6
J1301–6305 ¹	13:01:45.76(14)	–63:05:33.9(12)	51206	0.1845	266.747	374	11	7.1	6.6
J1341–6220 ⁴	13:41:42.63(8)	–62:20:20.7(5)	50859	0.1933	253.107	717.3	12.1	7.08	3.5
J1357–6429 ⁵	13:57:02.43(2)	–64:29:30.2(1)	52921	0.1661	360.1843	128.5	7.31	7.83	2.6
J1406–6121 ¹	14:06:50.04(6)	–61:21:27.9(6)	51111	0.2130	54.7010	537.8	61.7	3.45	6.5
J1413–6141 ³	14:13:09.87(9)	–61:41:13(1)	51500	0.2856	333.44	670.6	13.6	9.88	5.0
J1420–6048 ⁴	14:20:08.237(16)	–60:48:16.43(15)	51600	0.0681	83.1670	358.8	13.0	2.41	6.1
J1524–5625 ³	15:24:49.86(4)	–56:25:23.4(6)	51733	0.0782	38.9500	152.2	31.8	1.77	6.7
J1614–5048 ⁶	16:14:11.29(3)	–50:48:03.5(5)	50853	0.2316	494.943	582.4	7.42	10.8	6.1
J1646–4346 ⁷	16:46:50.8(3)	–43:45:48(8)	52792	0.2316	112.753	490.4	32.5	5.17	2.8
J1730–3350 ⁷	17:30:32.28(6)	–30:50:28(4)	53826	0.1394	84.8290	261.29	26.0	3.48	6.6
J1731–4744 ⁷	17:31:42.17(7)	–47:44:37(2)	54548	0.8298	163.626	123.056	80.4	0.11	6.7
J1830–1059 ²	18:30:47.566(10)	–10:59:27.9(6)	49621	0.4050	60.0250	159.70	107.0	4.99	4.2

References for parameters of these pulsars: 1 Manchester et al. (2001); 2 Hobbs et al. (2004); 3 Kramer et al. (2003); 4 Wang et al. (2000); 5 Lorimer et al. (2006); 6 D’Amico et al. (2001); 7 Yu et al. (2013).

the interval relative to glitch number in the first two columns. The next three columns list the spin parameters from fitting the spin-down models, including frequency (ν), first frequency derivative ($\dot{\nu}$) and second frequency derivative ($\ddot{\nu}$). The last four columns list reference epoch, fitted data span, number of ToAs and root mean square (RMS) residuals. Numbers in the parentheses indicate uncertainties in the last digit and correspond to 2σ from TEMPO2.

Glitch parameters (presented in Table A.1) were determined with two approaches that are extrapolation and phase-coherent timing fits. We extrapolated the pre-glitch and post-glitch solutions to the glitch epoch, and calculated the fractional jump in ν and $\dot{\nu}$. The results are given in the fourth and fifth columns, with uncertainties obtained by relying on standard error propagation equations. Columns seven to eleven give the values of glitch parameters from directly fitting Equation (2) with TEMPO2. The parentheses indicate the 1σ error in the last digit. The last three columns are the RMS of residuals, number of ToAs and data ranges. For glitch epochs appearing in the third column, they should be the halfway point of the last pre-glitch and first post-glitch observations, if we cannot obtain the only epoch by fitting with ToA data. Uncertainties for epochs are quoted to 1σ from TEMPO2 or half the observation gap. In addition, the second column gives a reference number which represents glitch number in this pulsar. The symbols Y and P in the sixth column are used to respectively denote if the glitch is new or has been reported.

Two types of figures are shown in the following sub-sections. One illustrates the spin frequency residuals and the spin frequency first time derivative with the values of ν and $\dot{\nu}$ obtained from independently fitting to short sections spanning 5 \sim 8 observations. The other one demonstrates timing residuals relative to the pre-glitch model that abruptly deflect downwards as an indicator of a small glitch. Each result is discussed in more detail in the following sub-sections.

3.1 PSR J0940–5428

In general, the rotation would exhibit irregularities for adolescence pulsars, which have characteristic ages less than ~ 100 kyr. PSR J0940–5428 has a relatively lower characteristic age $\tau_c \sim 42.2$ kyr and a similar period as Vela Pulsar, and, importantly, PSR J0940–5428 is a source of radio, X-ray and γ -ray radiations. Since 2001, no glitches have been observed in this pulsar at different frequency bands. In our data, phase coherency runs continuously for a long time until June 2010. To see whether it actually speeds up, we fitted the frequency ν and spin-down rate $\dot{\nu}$ to overlapping groups of ToA data, each of which typically covers a 50 d interval (Fig. 1). Clearly, there is not only an about 17853 nHz abrupt change in rotational frequency ν around MJD 55346 but also includes an exponential decay with timescale $\tau_d \sim 29$ d. From the fit of the glitch model, we derive the fraction of glitch recovery Q of 0.008(2). Besides, this giant glitch has a slow linear decay following the exponential relaxation.

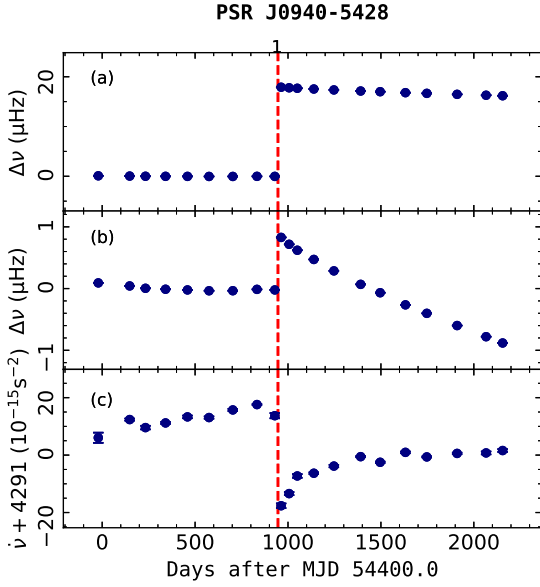


Fig. 1 The irregular rotation of PSR J0940–5428: (a) the variations in spin rate after subtracting the pre-glitch timing model. (b) same as (a) but the mean post-glitch frequency has been subtracted to reveal more detail and (c) the frequency derivative, $\dot{\nu}$. The red vertical dashed line tells the glitch epoch: 55346, and the number at the top of the graph signifies that this is the first glitch for this pulsar.

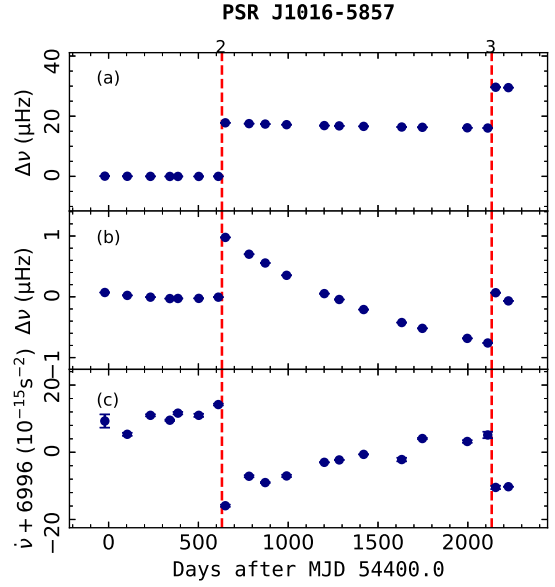


Fig. 3 Glitches of PSR J1016–5857: (a) the time-dependence of the frequency residuals $\Delta\nu$. (b) expanded plot of $\Delta\nu$ where the mean post-glitch value has been subtracted from the post-glitch data. (c) $\dot{\nu}$ around the time of the glitches. The red dashed lines are indicators of the time of glitch 2 and glitch 3: 55031 and 56533, and the number at the top of the graph signifies the sequence of glitches detected in this pulsar.

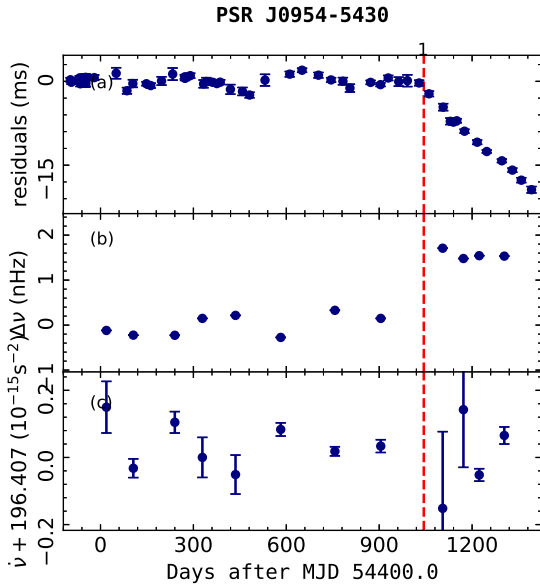


Fig. 2 One glitch in PSR J0954–5430: (a) variations in frequency obtained at glitch epoch relative to the pre-glitch solutions. (b) same as (a) but with the mean frequency of each side of the glitch epoch subtracted. (c) the variation of $\dot{\nu}$. The red dashed line marks a glitch detected in our data at MJD \sim 55444, and the number at the top of the graph signifies that this is the first glitch in this pulsar.

3.2 PSR J0954–5430

PSR J0954–5430 has a period of $P \sim 0.4728$ s and a characteristic age of $\tau_c \sim 171$ kyr. This pulsar has no known history of glitching. In our work, we released timing behaviors of PSR J0954–5430 derived from about 4.0 yr of timing observations at Parkes and show one small glitch in Figure 2. After fitting the glitch parameters for this glitch event, no exponential decay was observed. The fractional changes in frequency and frequency derivative are given in Table A.1.

3.3 PSR J1016–5857

PSR J1016–5857 has all the characteristics of a glitching pulsar, such as short period $P \sim 107$ ms, high period derivative $\dot{P} \sim 80 \times 10^{-15}$, relatively small characteristic age $\tau_c \sim 21$ kyr, and its spin-down luminosity of $\dot{E} \sim 2.6 \times 10^{36}$ erg s $^{-1}$ is large. Pulsars with these similar parameters are usually categorized as “Vela-like” pulsars. In spite of the limited number of glitches, “Vela-like” pulsars have a commonality of glitching behavior. Regular timing observations of PSR J1016–5857 began in May 1999. Since then, two glitches have been detected by Yu et al. (2013) with similar sizes to Vela’s. We revisited the glitch on MJD 55031 with more data, resulting in a

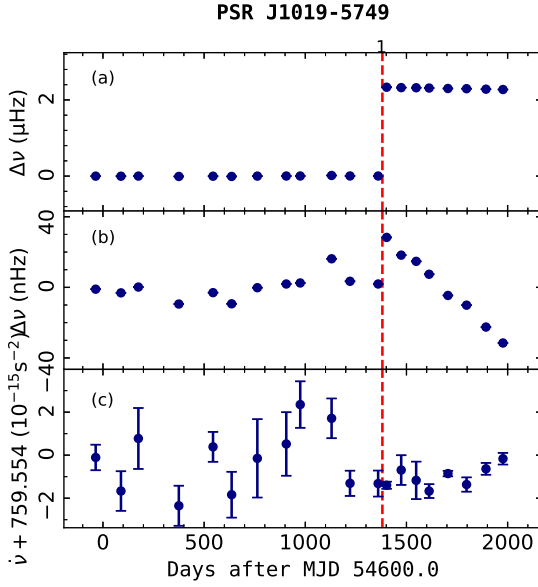


Fig. 4 The first new glitch in PSR J1019–5749. (a) the time-dependence of the frequency residuals $\Delta\nu$ relative to the pre-glitch spin-down solution. (b) expanded plot of $\Delta\nu$ where the mean post-glitch value has been subtracted from the post-glitch data. (c) $\dot{\nu}$ of pre-glitch and post-glitch. The vertical line splits our data into pre- and post-glitch sections. The glitch epoch is MJD ~ 55981 , and the top number signifies that this is the first glitch in this pulsar.

detection of exponential relaxation which was not reported by Yu et al. (2013). The exponential decay is well modeled with $Q = 0.0049(9)$ and $\tau_d = 32(6)$ d. A new glitch was detected to occur in August 2013 (MJD ~ 56533) with $\Delta\nu/\nu \sim 1.5 \times 10^{-6}$ and $\Delta\dot{\nu}/\dot{\nu} \sim 1.9 \times 10^{-3}$ (Fig. 3). However, the post-glitch behavior of this event cannot be well studied due to insufficient data availability. In fact, Camilo et al. (2001) considered that this pulsar was in the process of exponential recovery at discovery inception, according to the sign and magnitude of $\ddot{\nu}$. Furthermore, we noticed the differences in $\ddot{\nu}$ between pre- and post-glitch for glitch 2 in panel (c) of Figure 3; fitting gave $\ddot{\nu}_p \sim -246 \times 10^{-24} \text{ s}^{-3}$.

3.4 PSR J1019–5749

PSR J1019–5749, which has the largest DM value in its own direction (Guseinov et al. 2003), previously has not been observed to glitch. After studying timing residuals for this pulsar, we found that one glitch occurred around MJD 55981 (Fig. 4). As a result, the fractional change in frequency and first frequency derivative are $\Delta\nu/\nu \sim 378.3 \times 10^{-9}$ and $\Delta\dot{\nu}/\dot{\nu} \sim 1.39 \times 10^{-3}$, respectively. Panel (b) in Figure 4 displays the post-glitch behavior of spin frequency with a linear decay.

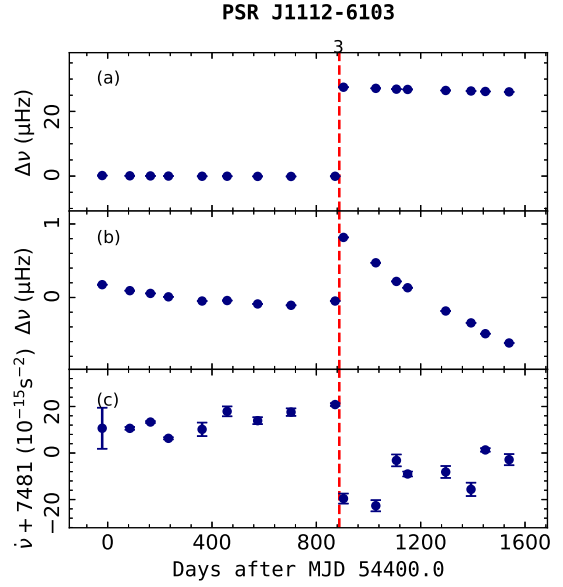


Fig. 5 Large glitch of PSR J1112–6103: (a) frequency residuals $\Delta\nu$ relative to the pre-glitch solution. (b) expanded plot of $\Delta\nu$ where the mean post-glitch value has been subtracted from the post-glitch data. (c) the frequency of first derivative $\dot{\nu}$. The red dashed line marks the glitch that occurred at MJD ~ 55288 , and the top number signifies that this is the third glitch in this pulsar.

3.5 PSR J1112–6103

The rotational characteristics for this pulsar suggest its timing behavior could be irregular, especially for a very small characteristic age $\tau_c \sim 32.7$ kyr and relatively large spin-down luminosity $\dot{E} \sim 4.5 \times 10^{36} \text{ erg s}^{-1}$. Indeed, large second time-derivative of the pulse frequency is an indicator of strong noise. Two large glitch events were detected by Yu et al. (2013). We report the latest 4.8 yr timing behavior of this pulsar. As shown in Figure 5, a new glitch occurred at MJD ~ 55288 . This event was a large glitch with glitch size $\Delta\nu/\nu \sim 1790.4 \times 10^{-9}$, corresponding to $\Delta\nu \sim 27\,569 \text{ nHz}$. There is no evidence of an exponential recovery. It is obvious that there is a permanent change in $\ddot{\nu}$ in the bottom panel of Figure 5; thus, we fitted a permanent increment of second frequency derivative with TEMPO2 to obtain the corresponding value $\Delta\ddot{\nu}_p \sim 113 \times 10^{-24} \text{ s}^{-3}$.

3.6 PSR J1248–6344

Until now, a pulsar glitch has not been detected in PSR J1248–6344, which has a greater characteristic age ($\tau_c \sim 186$ kyr) compared with most other glitching pulsars. The break in the timing residuals after MJD ~ 56075 implies the occurrence of a small glitch appearing in panel (a) of Figure 6. After modeling this glitch, the result of our

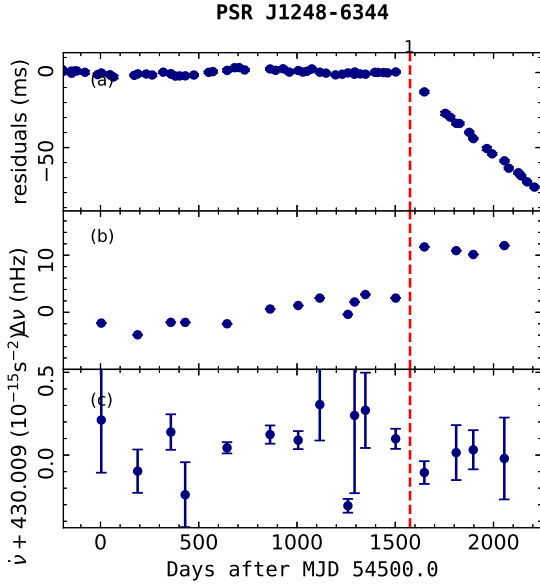


Fig. 6 The first glitch in PSR J1248–6344: (a) timing residuals derived from the pre-glitch timing model. (b) the sudden jump in the rotation frequency ν after glitch. (c) variations in frequency first derivative $\dot{\nu}$. The red vertical dashed line on the plot marks this glitch event around MJD 56075, and the top number signifies that this is the first glitch in this pulsar.

fit shows that relative change in the rotational frequency is $\Delta\nu/\nu \sim 1.6 \times 10^{-9}$, corresponding to the jump in frequency $\Delta\nu \sim 7.4$ nHz. This glitch does not exhibit significant change in its spin-down rate, and no exponential recovery was observed.

3.7 PSR J1301–6305

This $\tau_c \sim 11$ kyr PSR J1301–6305 is the fastest known pulsar (Sushch et al. 2017). In this work, over six years of observations were gathered to perform phase-coherent timing analysis. The timing residuals lost coherence due to a glitch occurring at MJD ~ 55124 . This event is large with a fractional change of frequency $\Delta\nu/\nu \sim 4158.4 \times 10^{-9}$ and frequency derivative $\Delta\dot{\nu}/\dot{\nu} \sim 4.93 \times 10^{-3}$ (Fig. 7). With regard to two previous large glitches, no exponential decay was reported. For this glitch, we report the post-glitch behavior exhibits an exponential decay, which has a fraction $Q \sim 0.0038(7)$ and timescale $\tau_d \sim 60(16)$ d. As is commonly observed in large glitches, this pulsar displays a linear increase in $\dot{\nu}$ after the exponential recovery.

3.8 PSR J1341–6220 (PSR B1338–62)

This pulsar is a good example of one displaying frequent glitches, and has so far been reported to suffer 23 glitches

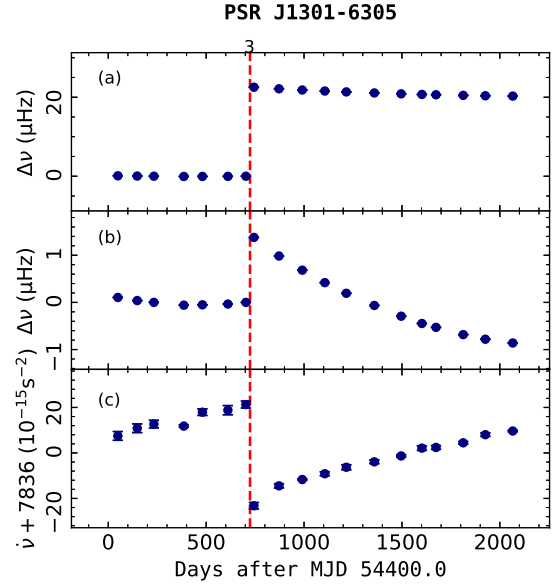


Fig. 7 A current glitch in PSR J1301–6305: (a) the frequency residuals relative to a simple slowdown model fitted to pre-glitch data. (b) expanded plot of $\Delta\nu$ where the mean post-glitch value has been subtracted from the post-glitch data. (c) the variations in $\dot{\nu}$. The red dashed line marks the glitch that occurred at MJD ~ 55124 , and the top number signifies that this is the third glitch in this pulsar.

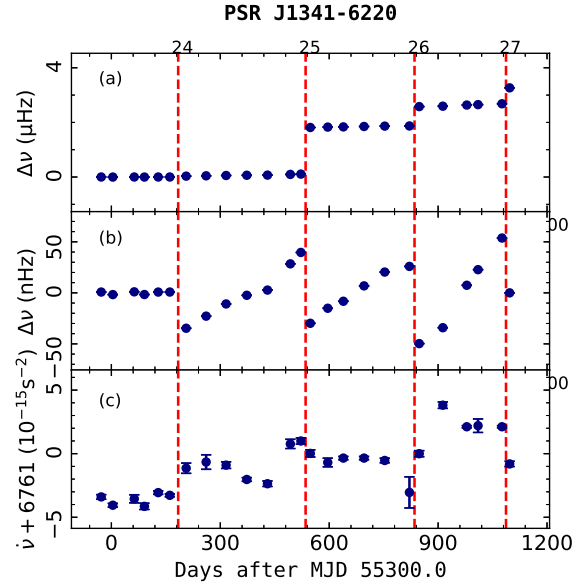


Fig. 8 Variations in ν and $\dot{\nu}$ for PSR J1341–6220: (a) an expanded $\Delta\nu$ after removal of ν and $\dot{\nu}$ just prior to the glitch. (b) an expanded plot of $\Delta\nu$ where the mean value has been removed from data after the marked glitches. (c) Observed variations in $\dot{\nu}$. Top numbers indicate the glitch number detected in this pulsar and vertical lines mark glitch epochs: 55491.1, 55835, 56135 and 56387.

Table 2 Pre- and post-glitch timing solutions. The inter-glitch braking indices n_{ig} are calculated as Eq. (8).

Pulsar Name (PSR)	Int.	ν (s^{-1})	$\dot{\nu}$ (10^{-12} s^{-2})	$\ddot{\nu}$ (10^{-24} s^{-3})	Epoch (MJD)	Range (MJD)	No. of ToAs	RMS μs	n_{ig}
J0940–5428	0–1	11.4212914643(2)	–4.278000(10)	78.1(14)	54816	54302–55330	42	1035	48.7(4)
	1–	11.4208508351(16)	–4.29170(4)	74(4)	56054	55363–56747	51	6414	28.3(8)
J0954–5430	0–1	2.11484087389(2)	–0.1963788(14)	–	54865	54302–55429	40	839	8(5)
	1–	2.11482796311(6)	–0.196392(16)	–	55626	55460–55792	12	355	244(147)
J1016–5857	1–2	9.3109884371(6)	–6.98631(2)	141(6)	54657	54302–55012	33	1365	26.9(6)
	2–3	9.3103268351(10)	–6.99766(2)	133(2)	55781	55050–56512	56	5881	23.1(3)
	3–	9.3098146172(6)	–7.0061(2)	–	56651	56555–56747	8	424	–
J1019–5749	0–1	6.0174063863(2)	–0.759402(4)	5.2(2)	55131	54302–55961	63	2392	55(1)
	1–	6.1535690535(2)	–0.76053(2)	–	56374	56002–56747	29	1855	118(20)
J1112–6103	2–3	15.3912863253(12)	–7.46752(4)	135(6)	54787	54303–55273	42	2331	37.4(8)
	3–	15.3907311759(10)	–7.48802(4)	283(8)	55689	55304–56075	51	1888	77(1)
J1248–6344	0–1	5.04183338973(4)	–0.429963(2)	–	55152	54303–56003	51	1434	9(5)
	1–	5.04178599437(18)	–0.42999(4)	–	56428	56148–56709	15	870	85(75)
J1301–6305	2–3	5.4169002952(4)	–7.82315(2)	246(4)	54703	54303–55104	30	2315	21.7(1)
	3–	5.4160738655(6)	–7.835854(16)	231.4(12)	55957	55144–56709	55	5213	19.9(2)
J1341–6220	23–24	5.1696641848(2)	–6.76443(18)	–	55321	55182–55462	18	266	0.09(7)
	24–25	5.1694637836(2)	–6.76206(12)	–	55664	55506–55823	25	1709	9(2)
	25–26	5.1692779604(2)	–6.76184(8)	–	55985	55848–56122	20	805	–4(1)
	26–27	5.1691168472(6)	–6.7586(2)	–	56262	56148–56377	14	1332	13(6)
	27–	5.1690187233(2)	–6.7618(4)	–	56431	56397–56467	6	98	–
J1357–6429	3–4	6.0174063863(10)	–13.01128(10)	2156(38)	55390	55205–55576	25	1549	76.6(6)
	4–	6.016862955(2)	–13.11067(12)	814(38)	55897	55647–56149	31	4353	28.5(6)
J1406–6121	0–1	4.6927625961(2)	–1.205316(4)	5.3(4)	55225	54303–56149	57	4481	17.2(6)
	1–	4.6926460531(2)	–1.20591(6)	–	56462	56213–56709	18	1391	50(21)
J1413–6141	7–8	3.4998750729(8)	–4.07737(2)	32(2)	55016	54303–55731	57	13958	6.7(2)
	8–9	3.4995503950(14)	–4.07790(12)	169(48)	55940	55759–56122	15	2366	35(5)
	9–10	3.4994059657(12)	–4.0782(2)	–	56352	56148–56556	14	6951	–23(5)
	10–	3.4992990483(12)	–4.0822(4)	–	56659	56578–56741	7	1255	–
J1420–6048	3–4	14.6625679630(4)	–17.82499(14)	1011(18)	54559	54303–54634	17	214	46.6(4)
	4–5	14.661853360(2)	–17.84925(14)	1547(26)	55031	54672–55392	44	4973	61.9(1)
	5–6	14.660623934(2)	–17.85505(10)	1008(14)	55841	55429–56255	37	3816	43.1(1)
	6–	14.659620572(2)	–17.8704(2)	1092(76)	56510	56279–56741	25	2015	38.3(7)
	0–1	12.7829149008(2)	–6.378549(6)	144.5(6)	55016	54303–55731	52	1120	45.4(1)
J1524–5652	1–	12.782272366(2)	–6.39875(10)	271(158)	56249	55759–56741	48	7624	63.0(1)
	2–3	4.312559294(4)	–9.17382(14)	298(20)	55275	54819–55731	30	22743	–15.2(5)
	3–4	4.311937555(6)	–9.1883(2)	2618(62)	56080	55739–56422	35	29309	133(1)
	4–	4.311548701(2)	–9.2021(4)	1133(178)	56603	56466–56741	14	3567	57(4)
J1646–4346	1–2	4.3166216098(8)	–2.09021(12)	101(4)	54788	54303–55273	34	5825	100(2)
	2–	4.3165158894(8)	–2.10832(4)	294(12)	55576	55304–55850	25	2587	286(6)
J1730–3350	2–3	7.1686768888(14)	–4.35662(2)	70(2)	55107	54303–55913	56	12349	26.7(4)
	3–	7.1682284068(16)	–4.37073(6)	127(12)	56340	55940–56741	34	4178	28(6)
J1731–4744	4–5	1.20498434273(2)	–0.2374408(12)	–	55016	54303–55731	52	2104	–7.8(4)
	5–6	1.20496449931(10)	–0.237660(18)	–	55986	55759–56215	20	2158	306(29)
	6–	1.20495402355(8)	–0.237486(14)	–	56497	56255–56741	17	1549	–139(26)
J1830–1059	1–2	2.46868786235(14)	–0.36565(2)	–	55440	55233–55648	14	940	–125(86)
	2–3	2.46867381648(12)	–0.36565(2)	–	55885	55696–56075	16	934	–32(82)
	3–4	2.46865952085(16)	–0.36541(2)	–	56338	56121–56557	15	1281	–202(69)
	4–	2.46864863919(18)	–0.36564(12)	–	56683	56627–56741	5	168	–

(Weltevrede et al. 2010; Yu et al. 2013). At Parkes, long-term regular and frequent observations had been built up. Figure 8 displays the evolution of ν and $\dot{\nu}$ in our ~ 3.5 yr data, where four new glitches are presented. Three of these events are medium glitches with $\Delta\nu/\nu \sim 1 - 3 \times 10^{-7}$ and feature a slight change in $\Delta\dot{\nu}/\dot{\nu}$. The other glitch is small with relative magnitude $\Delta\nu/\nu \sim 5 \times 10^{-9}$, and cannot be identified easily in Figure 8. There is no evidence for any exponential relaxations of spin frequency for all these glitches. However, rapid decays could have been easily missed because of the large gaps between observing sessions.

3.9 PSR J1357–6429

Two glitch events that occurred at MJDs ~ 52021 and ~ 54803 were previously detected for this very young pulsar (Weltevrede et al. 2010). Two years later, a new large glitch was discovered by Parkes. Figure 9 mirrors the instantaneous change in frequency ν and frequency derivative $\dot{\nu}$ around the epoch 55611. By fitting Equation (2) we are able to obtain the fractional change of ν and $\dot{\nu}$. The corresponding values are 4812×10^{-9} and 12.3×10^{-3} . There is some indication of exponential decay with long timescale.

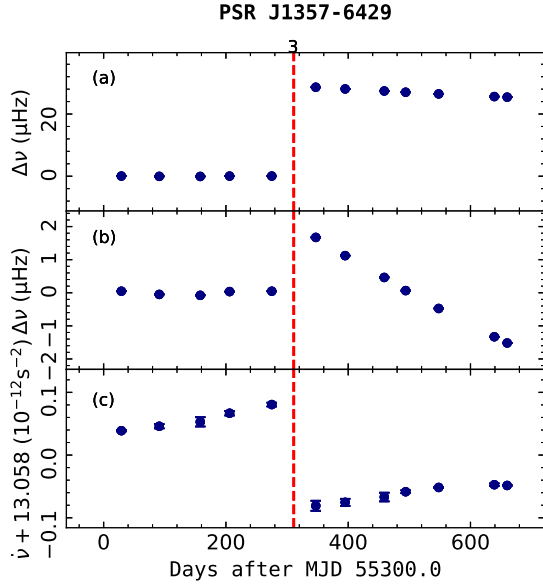


Fig. 9 A large glitch in PSR J1357–6429: (a) the time-dependence of the frequency residuals $\Delta\nu$ relative to the pre-glitch spin-down solution. (b) expanded plot of $\Delta\nu$ where the mean post-glitch value has been subtracted from the post-glitch data. (c) the frequency first derivative. The red line indicates the epoch at which the large glitch occurred at MJD ~ 55611 . Number 3 signifies that this is the third glitch in PSR J1357–6429.

3.10 PSR J1406–6121

PSR J1406–6121, which has a characteristic age $\tau_c = 61.7$ kyr and spin down energy loss rate $\dot{E} = 2.2 \times 10^{35}$ erg s $^{-1}$, is considered as a candidate of a glitching pulsar with high levels of timing noise. Large timing residuals arise suddenly near MJD 56181 owing to the occurrence of a large glitch. This is the first detection of a glitch event in this pulsar. Figure 10 shows that this glitch causes the fractional change of frequency $\Delta\nu/\nu \sim 2615.6 \times 10^{-9}$, as well as frequency derivative $\Delta\dot{\nu}/\dot{\nu} \sim 0.75 \times 10^{-3}$. We found no evidence of an exponential decay existing following this glitch.

3.11 PSR J1413–6141

Long-term timing observations at Parkes have revealed that the rotation of this 13.6 kyr pulsar is very unstable. Since 1998, glitches detected by the Parkes radio telescope have grown to seven in number. Figure 11 presents the evolution of ν and $\dot{\nu}$ for ~ 5 yr. During this period, this pulsar was found to undergo three new glitches. These glitches are medium, with $\Delta\nu/\nu \sim 2 \times 10^{-7}$. For the first of the three glitches, the second time-derivative of frequency $\ddot{\nu}$ dramatically changed after glitch, as usual

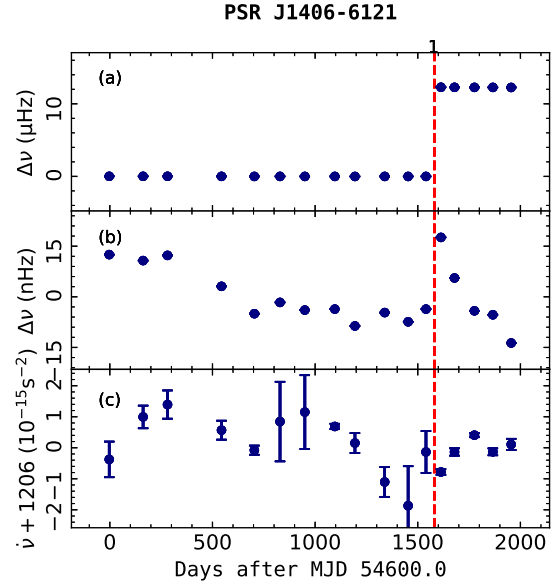


Fig. 10 Timing behaviors of PSR J1406–6121: (a) the spin rate after subtracting the pre-glitch timing model. (b) same as (a) but an offset is subtracted from the post-fit data and (c) the change of frequency first derivative $\dot{\nu}$. The top number and red dashed vertical line signify the first glitch around MJD 56202.

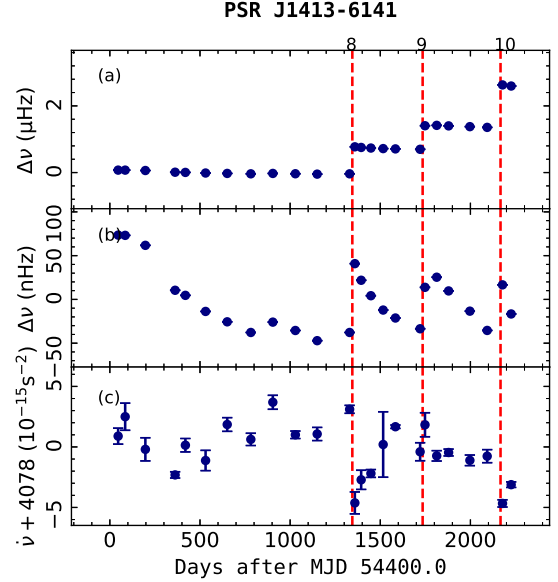


Fig. 11 Three medium glitches in PSR J1413–6141: (a) an expanded $\Delta\nu$ after removal of ν and $\dot{\nu}$ just prior to the glitch. (b) an expanded plot of $\Delta\nu$ where the mean value has been removed from data after the marked glitches. (c) the evolution of the frequency first derivative. The red dashed lines mark the glitch epochs: 55745, 56135 and 56567, and the number at the top of the graph signifies the sequence of glitches detected in this pulsar.

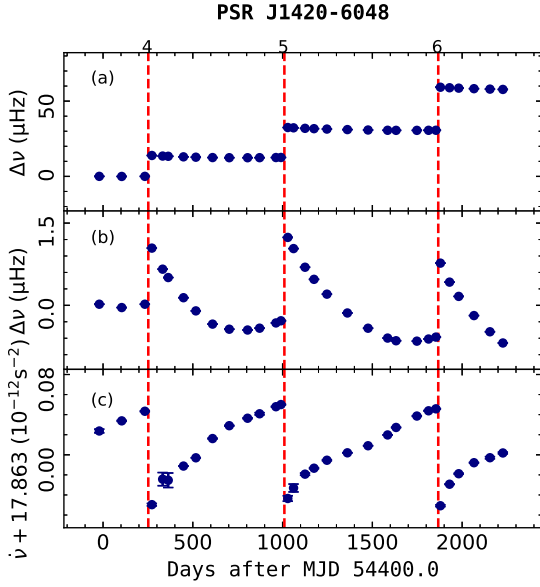


Fig. 12 The glitches of PSR J1420–6048: (a) the variations in spin rate after subtracting the pre-glitch timing model. (b) expanded plot of $\Delta\nu$ where the mean post-glitch value has been subtracted from the post-glitch data and (c) variations in frequency first derivative $\dot{\nu}$. The red vertical dashed lines mark the glitch epochs: 54652, 55410 and 56267, and the number at the top of the graph signifies the sequence of glitches detected in this pulsar.

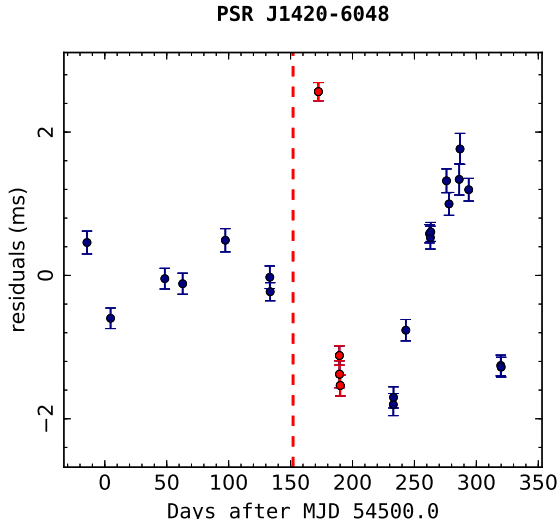


Fig. 13 Timing residuals for PSR J1420–6048 derived from fitting the five parameters: ν , $\dot{\nu}$, $\Delta\phi$, $\Delta\nu_p$ and $\Delta\dot{\nu}_p$. Red dots in the plot represent an exponential decay. The vertical dashed line signifies the assumed glitch epoch at MJD ~ 54652 .

for large glitches. The corresponding value of $\Delta\dot{\nu}_p$ is $158 \times 10^{-24} \text{ s}^{-3}$.

3.12 PSR J1420–6048

PSR J1420–6048 was discovered in October 1998 during the Parkes multibeam pulsar survey (D’Amico et al. 2001). D’Amico et al. (2001) pointed out that PSR J1420–6048 should be observed at higher frequencies, in accordance with the high spin-down energy flux $\dot{E}d^{-2}$. Mineo (2003) observed X-ray pulsation with ASCA observations and Nishida et al. (2003) confirmed γ -ray emission by the CANGAROO-II telescope from this young energetic rotation-powered pulsar. PSR J1420–6048 also displays irregularities. We were in the process of updating timing behaviors of this pulsar, and confirmed glitch 4 and glitch 5 detected by Yu et al. (2013) (Fig. 12). For glitch 4, Weltevrede et al. (2010) and Yu et al. (2013) reported no exponential decay for the post-glitch behavior. However, it is clear that there is a remarkable characteristic of an exponential recovery in timing residuals as presented in Figure 13, when we fitted Equation (2) to data spanning the glitch. This decay is characterized by $Q = 0.032(8)$ and $\tau_d = 91(24)$ d. Inadequate data availability had posed a significant obstacle to the study of post-glitch behavior for glitch 5 in the Yu et al. (2013) work. We analyzed follow-up observations of this glitch. The result affirms that there is an exponential decay with $Q = 0.0115(7)$ and $\tau_d = 89(6)$ d. Besides, we detected a new large glitch event. Our analysis indicates a fractional glitch size of $\Delta\nu/\nu \sim 1.9 \times 10^{-6}$, which makes it the largest glitch reported in this pulsar so far by a large margin. The relative change in spin down rate is $\Delta\dot{\nu}/\dot{\nu} \sim 4.15 \times 10^{-3}$. Fitting the timing phase residuals shows that the exponential timescale is 32(5) d, with $Q = 0.0079(9)$. In particular, there are clear indications of significant changes in $\dot{\nu}$ for all three glitches in panel (c) of Figure 12.

3.13 PSR J1524–5652

Most of the time, timing irregularities are particularly noticeable in younger pulsars. PSR J1524–5652 has a characteristic age $\tau_c \sim 31.8$ kyr. As expected, phase connection was lost near MJD 55745 because of a large glitch. This glitch causes the rotational frequency to increase to ~ 37830 nHz, as depicted in Figure 14. The relative change of magnitudes in frequency $\Delta\nu/\nu$ and frequency derivative $\Delta\dot{\nu}/\dot{\nu}$, which are obtained from fitting glitch parameters ν , $\dot{\nu}$, $\Delta\phi$, $\Delta\nu_p$ and $\Delta\dot{\nu}_p$, are 2949×10^{-9} and 5.6×10^{-3} respectively. Apparently, panels (b) and (c) in Figure 14 feature an exponential recovery for this event. The fitted value for the time constant τ_d of this exponential decay is about 100 d, with Q about 0.0076.

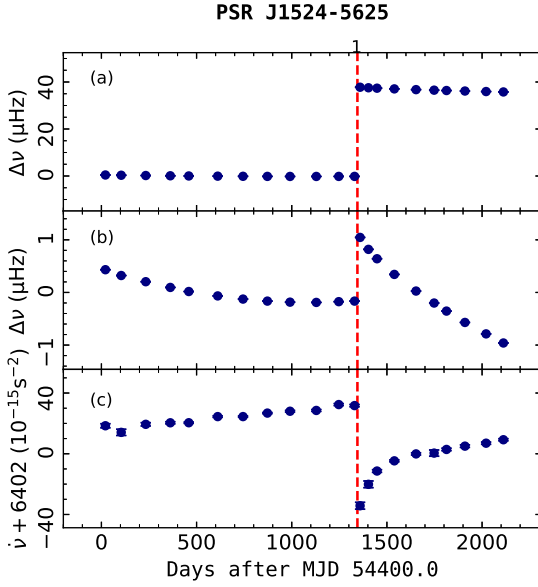


Fig. 14 The frequency and frequency derivative evolution of PSR J1524–5625. (a) the frequency residuals relative to a simple slowdown model fitted to pre-glitch data. (b) expanded plot of $\Delta\nu$ where the mean post-glitch value has been subtracted from the post-glitch data. (c) the variations in $\dot{\nu}$. The red dashed line marks the glitch that occurred at MJD ~ 55745 and the top number signifies that this is the first glitch in this pulsar.

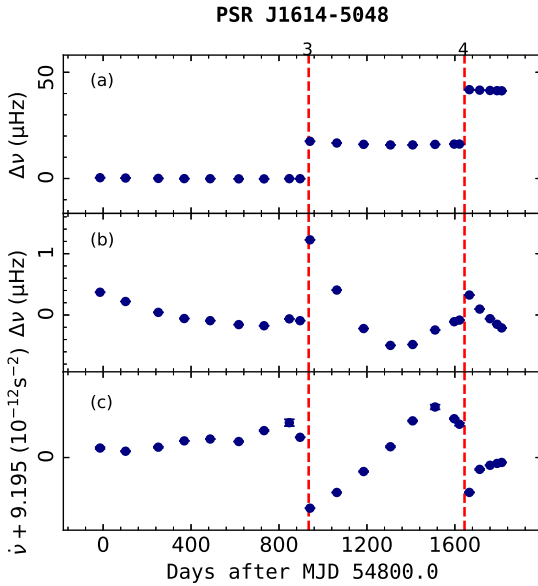


Fig. 15 Rotational frequency and first frequency derivative evolution for PSR J1614–5048: (a) the variations in spin rate after subtracting the pre-glitch timing model. (b) the mean post-glitch frequency has been subtracted to show more detail and (c) the frequency derivative, $\dot{\nu}$. The red vertical dashed lines mark the epochs of two glitches: 55735 and 56444, and the number at the top of the graph signifies the sequence of glitches detected in this pulsar.

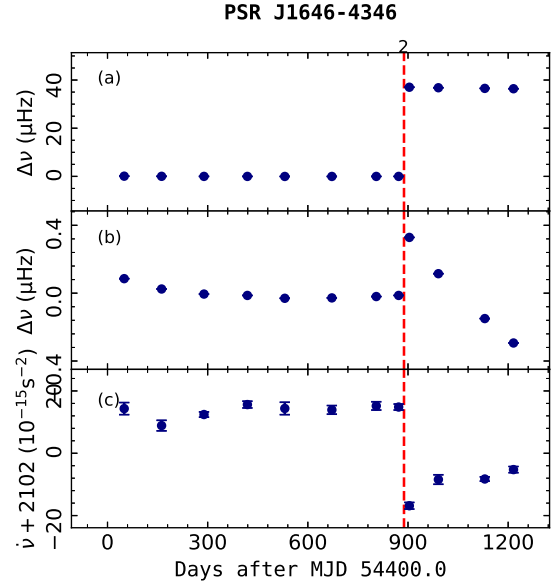


Fig. 16 The glitch of PSR J1646–4346: (a) variations in frequency residual $\Delta\nu$ relative to the pre-glitch value. (b) expanded plot of $\Delta\nu$ where the mean post-glitch value has been subtracted from the post-glitch data and (c) variations in frequency first derivative $\dot{\nu}$. The red dashed line marks the glitch that occurred at MJD ~ 55288 , and the top number signifies that this is the second glitch in this pulsar.

3.14 PSR J1614–5048

PSR J1614–5048 has a very small characteristic age of $\tau_c \sim 7.4$ kyr, which ranks it in 14th place among 188 known glitching pulsars. This pulsar also has a large spin down energy loss rate of $\dot{E} \sim 1.6 \times 10^{36}$ erg s $^{-1}$. For such a young and energetic pulsar, one of the important features is that it is very unstable, leading to difficulty in maintaining the phase being connected. Wang et al. (2000) suggested that the instability would result from inaccurate timing position, but Yu et al. (2013) attributed it to the effect of large-scale fluctuations in $\dot{\nu}$. Two large glitches had been published by Yu et al. (2013). Figure 15 also displays two very large glitches. Two events occurred separately at MJD ~ 55735 and ~ 56444 , corresponding to a fractional change in frequency $\Delta\nu/\nu \sim 4 \times 10^{-6}$ and 5.9×10^{-6} and a fractional change in frequency derivative $\Delta\dot{\nu}/\dot{\nu} \sim 8.87 \times 10^{-3}$ and 7.2×10^{-3} . Despite the variations in post-glitch $\dot{\nu}$, glitch 4 shows little characteristic of an exponential relaxation process. Rapid decays could have been easily missed because of the low-cadence timing observations.

3.15 PSR J1646–4346 (PSR B1643–43)

Johnston et al. (1992) discovered PSR J1646–4346 in high-frequency searching, which is located near the

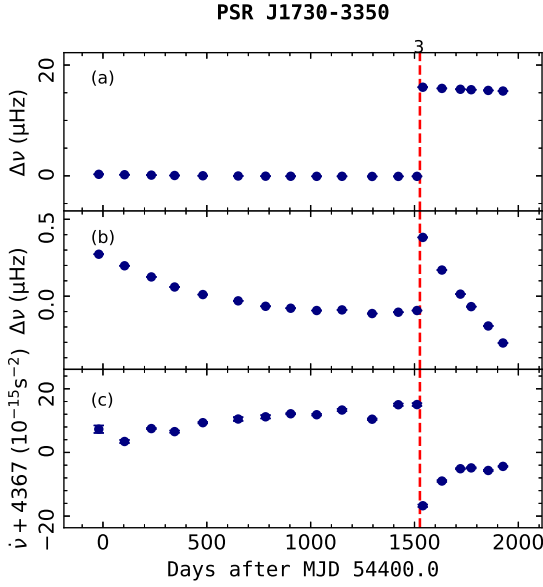


Fig. 17 The rotational parameters of PSR J1730–3350: (a) the time-dependence of the frequency residuals $\Delta\nu$ relative to the pre-glitch spin-down solution. (b) expanded plot of $\Delta\nu$ where the mean post-glitch value has been subtracted from the post-glitch data. (c) the frequency first derivative. The red line indicates the epoch at which the large glitch occurred at MJD ~ 55926 . Number 3 signifies that this is the third glitch in PSR J1730–3350.

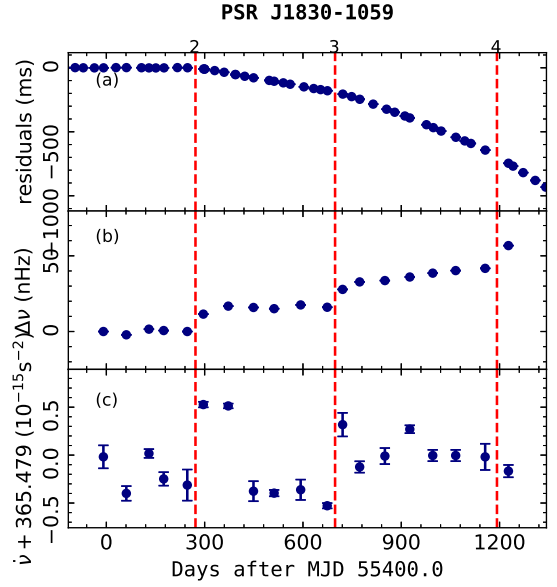


Fig. 19 ν and $\dot{\nu}$ evolution of PSR J1830–1059: (a) timing residuals relative to the pre-glitch model. (b) the variations in spin rate after subtracting the pre-glitch timing model. (c) variations in frequency first derivative. The red dashed lines are an indicator of the time of glitches 2, 3 and 4: 55672, 56120 and 56592, and the numbers at the top of the graph signify the sequence of glitches detected in this pulsar.

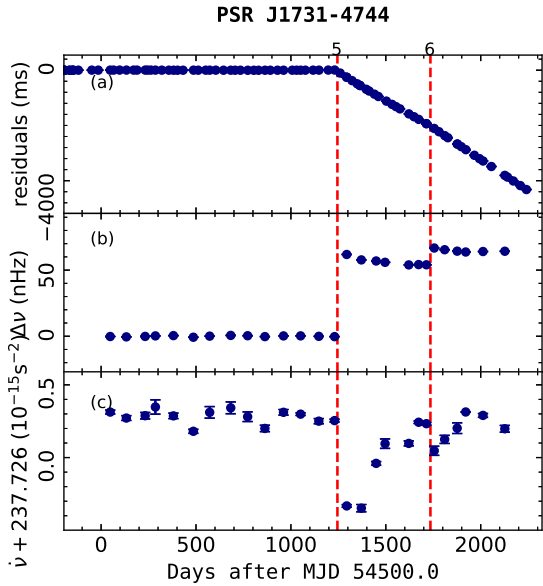


Fig. 18 Two small glitches in PSR J1731–4744: (a) timing residuals for glitch 5 and glitch 6 that occurred on MJD ~ 55745 and ~ 56235 respectively. (b) the variations in spin rate after subtracting the pre-glitch timing model. (c) the evolution of the frequency first derivative. The red dashed lines indicate the glitch epochs: 55745 and 56235, and the number at the top of the graph signifies the sequence of glitches detected in this pulsar.

Galactic centre. This pulsar is young and has a large spin-down luminosity ($\dot{E} > 10^{35}$ erg s $^{-1}$). We tracked the evolution of ν and $\dot{\nu}$ in Figure 16, and detected a new “giant” glitch at MJD ~ 55288 . According to Yu et al. (2013), this pulsar underwent a first glitch at MJD ~ 53875 with the fractional increase in pulsar rotation frequency $\Delta\nu/\nu \sim 885 \times 10^{-9}$. After nearly four years elapsed, this pulsar experienced a second abrupt increase in frequency with fractional size $\Delta\nu/\nu \sim 8584 \times 10^{-9}$ and change in frequency derivative with relative magnitude $\Delta\dot{\nu}/\dot{\nu} \sim 14.0 \times 10^{-3}$. The second glitch size is up to roughly ten times that of the first glitch. Specifically, there is a clear linear recovery after the large glitch, which is similar to the post-glitch behavior of the first event. This glitch causes a permanent change in $\ddot{\nu}$ with $\Delta\ddot{\nu}_p \sim 224 \times 10^{-24}$ s $^{-3}$.

3.16 PSR J1730–3350 (PSR B1727–33)

In Figure 17, we feature a large glitch at MJD ~ 55926 , with $\Delta\nu/\nu \sim 2.2 \times 10^{-6}$ and $\Delta\dot{\nu}/\dot{\nu} \sim 5 \times 10^{-3}$. This glitch is the third glitch in the pulsar, which had been mentioned in the Jodrell Bank Glitch Catalogue². The post-glitch behavior is a linear decay following the slight exponential relaxation. As is obvious in panel (c) of Figure 17, the post-glitch spin-down rate has a permanent

increase of $22.5(6) \times 10^{-15} \text{ s}^{-2}$. The exponential decay was modeled with $Q = 0.0065(3)$ and $\tau_d = 68(7) \text{ d}$.

3.17 PSR J1731–4744 (PSR B1727–47)

Glitch events are less frequent in PSR J1731–4744 relative to other glitching pulsars. Only four glitches have been reported by Yu et al. (2013) with $\Delta\nu/\nu$ between $\sim 10^{-7}$ and $\sim 10^{-9}$. Recently, a very large glitch at the epoch of MJD ~ 57984 was detected with $\Delta\nu/\nu \sim 3.1 \times 10^{-6}$ by the Molonglo Observatory Synthesis Radio Telescope and published in Astronomer’s Telegraph⁴. Figure 18 depicts two small glitches on MJD $\sim 55745(15)$ and $\sim 56235(21)$ which are not mentioned in previous publications. The former glitch is characterized by a fractional glitch size of $\Delta\nu/\nu \sim 5 \times 10^{-8}$. Fitting the glitch model to the timing residuals showed that the exponential timescale is $148(19) \text{ d}$, with $Q = 0.05(1)$. For the latter sudden jump, the fractional glitch size is five times lower than the former, and there is no a significant change in spin-down rate or an indication of exponential decay after this glitch.

3.18 PSR J1830–1059 (PSR B1828–11)

PSR J1830–1059 was recently added to the Jodrell Bank Glitch Catalogue as a new glitching pulsar. New measurement from Jodrell Bank Observatory indicated that a small glitch occurred at MJD ~ 55041.75 with $\Delta\nu/\nu \sim 6.2 \times 10^{-9}$ by using the Lovell telescope. However, we tend to count this timing behavior as timing noise from our data. Here, a plot (Fig. 19) of typical pulsar glitches is displayed. All three new glitches are small glitches with no or little change in $\dot{\nu}$ and correspond to the increase of $\nu \sim 12 \text{ nHz}$, 10 nHz and 12 nHz . Concrete glitch parameters are provided in Table A.1. No evidence for exponential decays are shown in Figure 19 or our fit processes.

4 DISCUSSION AND CONCLUSIONS

As presented in Section 3, a total of 30 glitches was detected in 18 pulsars, with timing observations from the 64-m Parkes radio telescope in Australia between 2007 and 2015. These pulsars are aged between 7.31 and 479 kyr. In our results, four reported glitches were revisited with updated exponential relaxations, and 26 new glitches were discovered. In particular, six pulsars were not previously known to glitch. Moreover, the distribution of $\Delta\nu/\nu$ is consistent with Yuan et al. (2010) and Yu et al. (2013), which is bimodal with peaks at approximately 10^{-6} and 10^{-9} (Fig. 20). All large glitches follow a few thousandths change in $\Delta\dot{\nu}/\dot{\nu}$, and a lower (one order

of magnitude) change appears in small glitches. For the post-glitch recoveries, most glitches exhibit a long-term linear recovery, and only nine exponential relaxations were observed in this work. These exponential decays occurred in large glitches with low Q , by just a few percent. Observed time constant τ_d for exponential recoveries ranged from 29 d to 148 d. Additionally, it is obvious that small glitches are common in relatively older pulsars, and all large glitches occur in young pulsars.

In summary, our work significantly increases the sample of known pulsar glitches and advances the understanding of properties of a glitch and the mechanism behind it. Here, we have sourced lists of glitches for 21 pulsars in Table A.2, including our work’s 18 pulsars and three other pulsars that have been reported to have an excess of 20 glitches, and discuss these two aspects in Section 4.1 and Section 4.2 respectively.

4.1 The Properties of Glitches

4.1.1 The rate of glitches \dot{N}_g

Glitch epoch and glitch amplitude of each glitch detected in each pulsar are given in Table A.2, to calculate the number of glitches per year \dot{N}_g and the uncertainty of \dot{N}_g derived from the square root of total number glitches dividing the data span. There are only three pulsars that exhibit glitches more than once per year, including PSR J0537–6910 with $\sim 3.6 \text{ yr}^{-1}$, PSR J1740–3015 with $\sim 1.21 \text{ yr}^{-1}$ and PSR J1341–6220 with $\sim 1.17 \text{ yr}^{-1}$. Ashton et al. (2017) firstly found the best fit with a linear function for the glitch rate based on Espinoza et al. (2011),

$$\langle \dot{N}_g \rangle = 10^{-3.00} |\dot{\nu}|^{0.47} 10^{\pm 0.31} \text{ s}^{-1}. \quad (4)$$

We also give the values of $\langle \dot{N}_g \rangle$ in Table A.2. Comparing \dot{N}_g with $\langle \dot{N}_g \rangle$, it seems that this formula is applicable for the less frequently glitching pulsars.

4.1.2 Glitch activity A_g

We reported the glitch activity in the sixth column of Table A.2, which is an approach to quantify the contribution of glitches to $\dot{\nu}$ (Yuan et al. 2010) and the cumulative effects of a collection of spin-ups (Fuentes et al. 2017). The glitch activity parameter was firstly introduced by McKenna & Lyne (1990) as

$$A_g = \frac{1}{T} \sum \frac{\Delta\nu}{\nu}, \quad (5)$$

where $\sum \frac{\Delta\nu}{\nu}$ is the sum of every fractional change in ν of every glitch for each pulsar, and T is the total time taken to search for glitches. Our results are consistent with previous statistical analysis that Espinoza et al. (2011) performed

⁴ <http://www.astronomerstelegam.org>

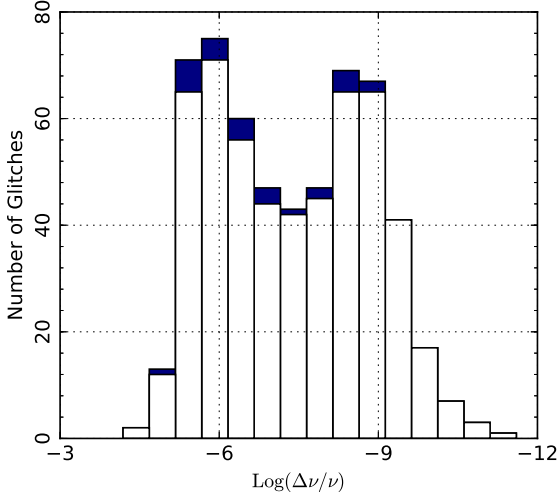


Fig. 20 Histogram of the distribution of fractional glitch amplitude $\Delta\nu/\nu$. The blank bars correspond to results from the previous work, while the blue bars signify new detections from this work. For previously reported glitches, we referenced the Jodrell Bank Glitch Catalogue².

with a conclusion that A_g decreases in pulsars with low spin-down rate. However, PSR J0534+2200 has the largest spin-down rate of $|\dot{\nu}| \sim 377 \times 10^{-12} \text{ s}^{-2}$, and it exhibits a small $A_g \sim 0.21 \times 10^{-7} \text{ yr}^{-1}$ in our sample. Here, $A_g \sim 9.13 \times 10^{-7} \text{ yr}^{-1}$ in PSR J1614–5048 provides evidence to group it into a class of the most frequently glitching pulsars. Urama & Okeke (1999) analyzed a total of 71 glitches in 30 pulsars and found a very good correlation of A_g with $|\dot{\nu}|$ for characteristic ages older than 10^4 yr , which can be described by,

$$A_g \approx 41.4 + 3.22 \log |\dot{\nu}|, \quad (6)$$

where A_g is in the unit of 10^{-7} yr^{-1} . This relationship can be used to predict the glitch activity for these glitching pulsars in Table A.2. The values that we obtained are in good agreement (± 1) with observational values except for PSR J1830–1059. Glitch activity in PSR J1830–1059 is much lower than predicted, possibly due to some missed small glitches in the previous timing observations.

4.1.3 Glitch waiting time

Glitch events are considered occurring with a known constant rate and independently of the time since the previous glitch (Wang et al. 2012; Shaw et al. 2018). Then, a reasonable assumption is that the mean waiting time λ of a new glitch occurring obeys a Poissonian probability density distribution

$$P(t) = 1 - e^{-t/\lambda}. \quad (7)$$

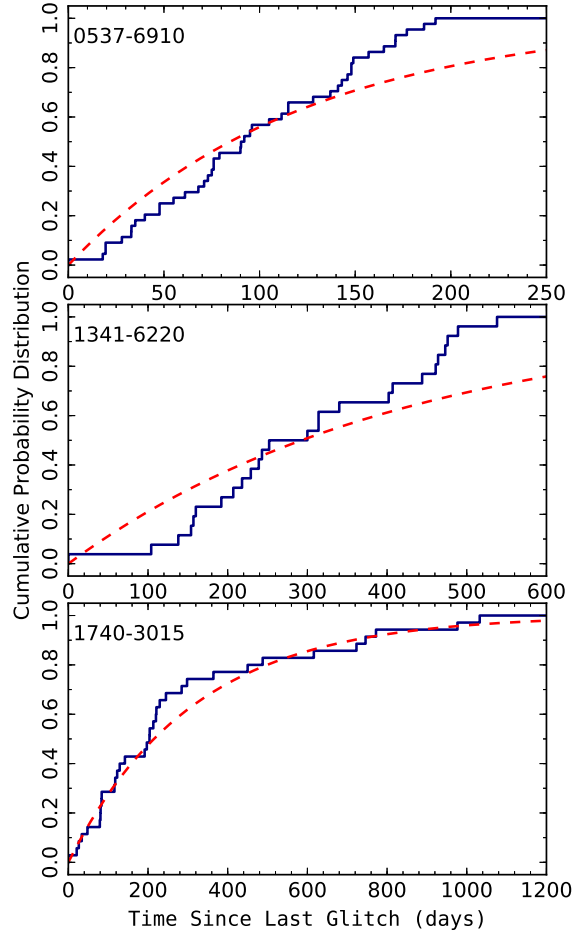


Fig. 21 Cumulative probability distribution of inter-glitch intervals for PSRs J0537–6910, J1341–6220 and J1740–3015. The red dashed curves represent Poisson distributions with mean waiting times of 122 d, 422 d and 310 d for a glitch, respectively.

For PSR J0534+2200, the cumulative distribution of glitch waiting times is in good agreement with the Poisson model (Shaw et al. 2018). Here, Figure 21 displays the cumulative probability distribution and fitted results of the Poisson model for the three most frequently glitching pulsars in our sample. The mean waiting times for PSRs J0537–6910, J1341–6220 and J1740–3015 are 122 d, 422 d and 310 d, respectively. Kolmogorov-Smirnov (K-S) tests for our data of three pulsars based on Poisson model all show that the Poisson model should be rejected with a P-value of about 13%, 9.5% and 74%, respectively.

4.2 Implications for Neutron-Star Physics

4.2.1 Braking index

According to classical electrodynamics, pulsars can lose their rotational kinetic energy in the forms of high energy particle outflow or low-frequency electromagnetic waves. Therefore, pulsars can gradually slow down. These physical processes are considered associated with the pulsar magnetosphere which determines the electromagnetic radiation generation. In this case, the braking index can be expressed by

$$n = \frac{\ddot{\nu}\nu}{\dot{\nu}^2}. \quad (8)$$

So if ν , $\dot{\nu}$ and $\ddot{\nu}$ are given, the braking index n can be calculated. Typically, the braking index n is equal to 3 with magnetic dipole radiation (Livingstone et al. 2007). Now we measure the pre- and post-glitch braking indices (which skips the post-glitch exponential decay) for each pulsar based on the timing solutions and give the results in the last column of Table 2. These values are highly variable between different pulsars and different intervals of a glitch, ranging between -202 and 306 , but they still make sense in that glitches would originate from the internal dynamics of a neutron star rather than the magnetosphere.

4.2.2 The fractional moment of inertia

Based on angular momentum exchange models, Ravenhall & Pethick (1994) firstly demonstrated an approximate expression for the crust fractional moment of inertia (FMI). Subsequently, Link et al. (1999) suggested that glitches represent a self-regulated process that involves a superfluid reservoir with moment of inertia, which is described by the following equation (Andersson et al. 2012)

$$\frac{I_n}{I} \approx 2\tau_c \frac{1}{t_{\text{obs}}} \left(\sum_i \frac{\Delta\Omega_p^i}{\Omega_p} \right), \quad (9)$$

where the left-hand side of the above equation is the ratio of the superfluid component I_n and the moment of inertia of the entire star I . The FMI associated with glitches should be at least $1 \sim 1.5\%$, both from observation and theory (Link et al. 1999; Andersson et al. 2012). Piekarewicz et al. (2014) suggested that the superfluid reservoir in the crust is enough to produce the observed glitch sizes. Here, we calculated FMI for 14 pulsars which have underwent at least two large glitches in Table A.2. Some cases are less impressive due to only a few glitches occurring, but the results still agree with the conclusions of Link et al. (1999) and Piekarewicz et al. (2014).

We close this paper by looking forward to the future of studying pulsar glitches. Although so many

glitches have been detected in different young pulsars, the reason for pulsar glitches remains unknown. Obviously, persistent pulsar timing observations should be carried out. Furthermore, the new generation Five-hundred-meter Aperture Spherical Radio Telescope (FAST) has commenced timing observations of pulsars, and we can expect an improved understanding of the properties of glitches and neutron-star interiors.

Acknowledgements The Parkes radio telescope is part of the Australia Telescope, which is funded by the Commonwealth of Australia for operation as a National Facility managed by the Commonwealth Scientific and Industrial Research Organisation (CSIRO). Our work is supported by the National Natural Science Foundation of China (Nos. 11273020, U1731111 and 11847048), the Sichuan Provincial Department of Science and Technology Project (No. 2018JY0502) and the Fundamental Research Funds of China West Normal University (No. 20B009). We would like to express our gratitude to everyone who contributed to make this study possible.

Appendix A: TIMING SOLUTIONS AND GLITCH PARAMETERS

Glitch parameters are listed in Table A.1 with two methods: extrapolating timing solutions and phase-coherent timing fits. Table A.2 summarizes observed glitches of 21 glitching pulsars for discussing the properties of these glitches and implications for neutron-star physics.

References

- Alpar, M. A., Anderson, P. W., Pines, D., & Shaham, J. 1981, ApJL, 249, L29
- Anderson, P. W., & Itoh, N. 1975, Nature, 256, 25
- Andersson, N., Glampedakis, K., Ho, W. C. G., & Espinoza, C. M. 2012, Phys. Rev. Lett., 109, 241103
- Antonopoulou, D., Espinoza, C. M., Kuiper, L., & Andersson, N. 2018, MNRAS, 473, 1644
- Archibald, R. F., Kaspi, V. M., Ng, C. Y., et al. 2013, Nature, 497, 591
- Ashton, G., Prix, R., & Jones, D. I. 2017, Phys. Rev. D, 96, 063004
- Camilo, F., Bell, J. F., Manchester, R. N., et al. 2001, ApJL, 557, L51
- Cognard, I., & Backer, D. C. 2004, ApJL, 612, L125
- Şaşmaz Muş, S., Aydın, B., & Göğüş, E. 2014, MNRAS, 440, 2916
- D’Amico, N., Kaspi, V. M., Manchester, R. N., et al. 2001, ApJL, 552, L45
- Dib, R., & Kaspi, V. M. 2014, ApJ, 784, 37
- Edwards, R. T., Hobbs, G. B., & Manchester, R. N. 2006, MNRAS, 372, 1549

Table A.1 Observed Glitch Parameters

Pulsar Name	Gl. No.	Epoch MJD	Extrapolated			New? (Y/P)	Fitted			Q	τ_d (d)	Res μ s	No. of ToAs	Data Range MJD
			$\Delta\nu/\nu$ (10^{-9})	$\Delta\dot{\nu}/\nu$ (10^{-3})	$\Delta\nu/\nu$ (10^{-9})		$\Delta\dot{\nu}/\nu$ (10^{-3})	$\Delta\dot{\nu}_p$ (10^{-15} s^{-2})						
J0940–5428	1	55346(17)	1563.2(3)	5.07(3)	Y	1564.2(2)	4.72(3)	–20.2(1)	0.008(2)	29(6)	408	30	55010 – 55697	
J0954–5430	1	55444(16)	0.67(6)	0.07(4)	Y	0.75(9)	–	–	–	–	388	22	55103 – 55792	
J1016–5857	2	55031(20)	1912.4(2)	3.50(1)	P	1912.8(2)	3.29(7)	–23.0(4)	0.0049(9)	32(6)	425	35	54672 – 55429	
	3	56533(22)	1459.4(2)	2.45(2)	Y	1463.4(3)	1.82(9)	–12.7(6)	–	–	788	20	56147 – 56747	
J1019–5749	1	55981(21)	376.7(1)	1.99(2)	Y	378.3(2)	1.39(9)	–1.05(7)	–	–	1052	30	55616 – 56327	
J1112–6103	3	55288(16)	1791.2(2)	4.82(2)	Y	1790.4(3)	6.1(1)	–45.6(9)	–	–	936	37	54858 – 55697	
J1248–6344	1	56075(73)	1.47(9)	0.07(3)	Y	1.6(1)	–	–	–	–	754	34	55461 – 56709	
J1301–6305	3	55124(21)	4158.5(3)	4.87(1)	Y	4158.4(8)	4.93(3)	–38.5(2)	0.0038(7)	60(16)	2125	48	54379 – 55648	
J1341–6220	24	55491.1(8)*	5.2(1)	–0.350(9)	Y	5.2(1)	–0.392(9)	2.65(6)	–	–	209	25	55304 – 55648	
	25	55835(13)	331.9(2)	–0.03(1)	Y	329.5(1)	0.21(1)	–1.4(1)	–	–	292	24	55696 – 56003	
	26	56135(14)	131.8(2)	–0.47(1)	Y	147.5(2)	–0.48(1)	3.2(1)	–	–	1064	32	55896 – 56377	
	27	56387(11)	111.3(3)	0.46(3)	Y	95.9(1)	0.42(3)	–2.8(2)	–	–	131	14	56254 – 56467	
J1357–6429	3	55611(36)	4792(9)	12.23(4)	Y	4812(5)	12.3(1)	–159(2)	–	–	1524	38	55363 – 55912	
J1406–6121	1	56181(33)	2615.5(2)	0.86(2)	Y	2615.6(3)	0.75(5)	–	–	–	2367	34	55696 – 56708	
J1413–6141	8	55445(15)	229(1)	1.3(1)	Y	232.0(4)	1.84(8)	–7.5(3)	–	–	860	26	55363 – 56075	
	9	56135(14)	203(1)	0.7(1)	Y	209(1)	0.08(4)	–0.3(2)	–	–	6409	29	55759 – 56556	
	10	56567(12)	368.4(9)	0.98(7)	Y	371(1)	0.7(1)	–3.1(5)	–	–	1730	13	56397 – 56741	
J1420–6048	4	54652(20)	948.4(4)	4.64(2)	P	910(9)	2.5(3)	–45(5)	0.032(8)	91(24)	137	23	54504 – 54821	
	5	55410(19)	1352.0(5)	5.25(2)	P	1348(1)	4.18(6)	–74(1)	0.0115(7)	89(6)	143	33	55182 – 55731	
	6	56267(12)	1948.7(6)	4.21(4)	Y	1944.0(5)	4.15(8)	–73(1)	0.0079(9)	32(5)	597	32	55960 – 56672	
J1524–5652	1	55745(15)	2959.5(4)	6.41(5)	Y	2949(1)	5.6(1)	–35(2)	0.0076(3)	100(5)	531	45	55363 – 56280	
J1614–5048	3	55735(5)	4099(2)	11.2(1)	Y	4097.4(4)	8.87(8)	–81.4(7)	–	–	738	26	55506 – 55961	
	4	56444(23)	5878(3)	12.1(1)	Y	5941(2)	7.2(2)	–66(2)	–	–	2673	26	56173 – 56741	
J1646–4346	2	55288(16)	8579.7(6)	14.11(9)	Y	8584(1)	14.0(4)	–29.2(9)	–	–	2230	30	54902 – 55648	
J1730–3350	3	55926(14)	2238.0(6)	5.41(5)	P	2236(1)	5.1(1)	–22.5(6)	0.0065(3)	68(7)	231	26	55647 – 56215	
J1731–4744	5	55745(15)	50.2(1)	0.92(4)	Y	49.6(4)	0.72(8)	–0.17(2)	0.05(1)	148(19)	299	25	55411 – 56079	
	6	56235(21)	10.8(2)	–0.73(5)	Y	10.8(2)	–0.73(5)	–0.17(1)	–	–	2006	37	55759 – 56741	
J1830–1059	2	55672(25)	5.2(1)	–0.01(6)	Y	5.2(1)	–	–	–	–	911	31	55233 – 56075	
	3	56120(4)*	4.4(1)	–0.65(5)	Y	4.4(1)	–0.65(6)	0.23(2)	–	–	1116	32	55696 – 56557	
	4	56592(36)	5.0(2)	0.6(1)	Y	4.7(8)	–	–	–	–	654	10	56421 – 56741	

* Glitch epoch determined by phase fit.

- Espinoza, C. M., Lyne, A. G., Stappers, B. W., & Kramer, M. 2011, *MNRAS*, 414, 1679
- Eya, I. O., Urama, J. O., & Chukwude, A. E. 2017, *ApJ*, 840, 56
- Folkner, W. M., Williams, J. G., & Boggs, D. H. 2009, *Interplanetary Network Progress Report*, 42–178, 1
- Fuentes, J. R., Espinoza, C. M., Reisenegger, A., et al. 2017, *A&A*, 608, A131
- Guseinov, O. H., Yazgan, E., Özkan, S., Sezer, A., & Tagieva, S. 2003, *Astronomical and Astrophysical Transactions*, 22, 301
- Hobbs, G. B., Edwards, R. T., & Manchester, R. N. 2006, *MNRAS*, 369, 655
- Hobbs, G., Lyne, A. G., Kramer, M., Martin, C. E., & Jordan, C. 2004, *MNRAS*, 353, 1311
- Hobbs, G., Miller, D., Manchester, R. N., et al. 2011, *PASA*, 28, 202
- Hotan, A. W., van Straten, W., & Manchester, R. N. 2004, *PASA*, 21, 302
- Johnston, S., Lyne, A. G., Manchester, R. N., et al. 1992, *MNRAS*, 255, 401
- Kou, F. F., Yuan, J. P., Wang, N., Yan, W. M., & Dang, S. J. 2018, *MNRAS*, 478, L24
- Kramer, M., Bell, J. F., Manchester, R. N., et al. 2003, *MNRAS*, 342, 1299
- Link, B., Epstein, R. I., & Lattimer, J. M. 1999, *Phys. Rev. Lett.*, 83, 3362
- Livingstone, M. A., Kaspi, V. M., Gavriil, F. P., et al. 2007, *Ap&SS*, 308, 317
- Lorimer, D. R., Faulkner, A. J., Lyne, A. G., et al. 2006, *MNRAS*, 372, 777
- Lower, M. E., Bailes, M., Shannon, R. M., et al. 2020, *MNRAS*, 494, 228
- Lyne, A. G., Shemar, S. L., & Smith, F. G. 2000, *MNRAS*, 315, 534
- Manchester, R. N., Lyne, A. G., Camilo, F., et al. 2001, *MNRAS*, 328, 17
- Manchester, R. N., Hobbs, G., Bailes, M., et al. 2013, *PASA*, 30, e017
- McKee, J. W., Janssen, G. H., Stappers, B. W., et al. 2016, *MNRAS*, 461, 2809
- McKenna, J., & Lyne, A. G. 1990, *Nature*, 343, 349
- Mineo, T. 2003, *The Hard X-Ray Emission of PSR J1420–6048*, *RXTE Proposal*
- Nishida, D., Kubo, H., Tanimori, T., et al. 2003, in *International Cosmic Ray Conference*, 4, 2489
- Palfreyman, J., Dickey, J. M., Hotan, A., Ellingsen, S., & van Straten, W. 2018, *Nature*, 556, 219
- Piekarewicz, J., Fattoyev, F. J., & Horowitz, C. J. 2014, *Phys. Rev. C*, 90, 015803
- Pizzochero, P. M., Antonelli, M., Haskell, B., & Seveso, S. 2017, *Nature Astronomy*, 1, 0134

Table A.2 List for All Glitches that had been Reported for 21 Pulsars

Pulsar NameInt. (PSR)	Glitch Epoch ($\Delta\nu/\nu$) MJD	\dot{N}_g (yr^{-1})	$\langle \dot{N}_g \rangle$ (yr^{-1})	$A_g (\times 10^{-7} \text{yr}^{-1})$		I_n/I	
				Observed	Predicted		
J0940–5428 1	55346(1564.2)	–	–	–	–	–	
J0954–5430 1	55444(16)	–	–	–	–	–	
J1016–5857 3	52549(1622.6), 55031(1912.8), 56533(1463.4)	0.27(15)	0.08	→ 0.36	3.45	5.48	1.92%
J1019–5749 1	55981(378.3)	–	–	–	–	–	
J1112–6103 3	51395(1825), 53337(1202), 55288(1790.4)	0.28(16)	0.09	→ 0.37	2.98	5.57	2.95%
J1248–6344 1	56075(1.6)	–	–	–	–	–	
J1301–6305 3	51923(4630), 53383(2664), 55124(4158.4)	0.34(19)	0.09	→ 0.38	7.24	5.63	2.87%
J1341–6220 27	47989(1509), 48453(23), 48645(996), 49134(13), 49363(146), 49523(37), 49766(15) 49904(31), 50008(1648), 50322(30), 50529(23), 50683(708), 51144(170), 51617(1121.5) 52093(480), 52250(454.5), 52788(219.2), 53232(277), 53471(985), 54128(194) 54468(316.1), 54870(300), 55088(1435), 55491.1(5.2), 55835(329.5), 56135(147.5) 56387(95.9)	1.17(22)	0.08	→ 0.36	3.55	5.43	1.23%
J1357–6429 3	52021(2428), 54803(1752), 55611(4812)	0.30(17)	0.11	→ 0.49	7.90	6.34	1.15%
J1406–6121 1	56181(2615.6)	–	–	–	–	–	
J1413–6141 10	51290(39), 51463(970), 51796.3(59.7), 52092(811), 52899.4(46.9), 53125(1410) 54288(2409.8), 55745(232.0), 56135(209), 56567(371)	0.69(21)	0.06	→ 0.28	4.09	4.13	1.23%
J1420–6048 6	51600(1146.2), 52754(2019), 53725(1270), 54652(910), 55410(1348), 56267(1944.0)	0.46(19)	0.13	→ 0.57	5.59	6.79	1.75%
J1524–5652 1	55745(2949)	–	–	–	–	–	
J1614–5048 5	49803(6460), 53013(6242), 55735(4097.4), 56444(5941)	0.21(10)	0.10	→ 0.41	9.13	–	1.81%
J1646–4346 2	53876(885), 55288(8584)	0.51(36)	0.05	→ 0.20	4.34	3.80	15.89%
J1730–3350 3	48000(3033), 52107(3202), 55926(2236)	0.13(7)	0.07	→ 0.29	3.50	4.82	2.01%
J1731–4744 7	49387.2(137), 50718.1(4.4), 52472.7(126.4), 53582(2.7), 55745(49.6) 56235(10.8), 57984(3147.7)	0.29(11)	0.01	→ 0.07	0.71	0.74	5.49%
J1830–1059 4	55041.75(6.2), 55672(5.2), 56117(4.4), 56592(4.7)	0.94(47)	0.02	→ 0.09	0.0041	1.35	–
J0534+2200 27	40491.8(7.2), 41161.98(1.9), 41250.32(2.1), 42447.26(35.7), 46663.69(6) 47767.504(81), 48945.6(4.2), 50020.04(2.1), 50260.031(31.9), 50458.94(6.1) 50489.7(0.8), 50812.59(6.2), 51452.02(6.8), 51740.656(25.1), 51804.75(3.5) 52084.072(22.6), 52146.7580(8.9), 52498.257(3.4), 52587.2(1.7), 53067.078(214) 53254.109(4.9), 53331.17(2.8), 53970.1900(21.8), 54580.38(4.7), 55875.5(49.2) 58064.555(471), 58237.357(4.08)	0.55(10)	0.57	→ 2.39	0.21	–	0.46%
J0537–6910 45	51286(681), 51569(449), 51711(315), 51826(140), 51881(141), 51960(456), 52152(2.4) 52171(185), 52242(427), 52386(168), 52453(217), 52545(421), 52740(144), 52819(256) 52887(234), 53014(338), 53125(18), 53145(392), 53288(395), 53446(259), 53551(322) 53699(402), 53860(236), 53951(18), 53999(352.09), 54080(370.99), 54243(0.9) 54268(489.05), 54449(239.91), 54538(113.74), 54576(147.39), 54628(132.5) 54712(106), 54765(362), 54891(341.84), 55045(216.43), 55183.6(208.42), 55242(552.8) 55445(171), 55507(124.4), 55556(9.8), 55587(87.2), 55619(453.2), 55786.1(14) 55815(316)	3.6(5)	0.42	→ 1.77	6.26	–	0.91%
J1740–3015 36	46991(421), 47289(31), 47337(7), 47466(26), 47670.22(600), 48158(10), 48191.69(659) 48218(48), 48431.3(16), 49047.5(17), 49239.07(169.7), 49459(10), 49542.3(6) 50574.83(442.5), 50939(1444), 51685(0.7), 51827(0.9), 52048(2), 52245(4), 52266(16) 52346.6(158), 52576(0.9), 52779.7(1.7), 52858.78(18.6), 52942.5(20.2) 53023.52(1850.9), 53473.56(0.8), 54450.19(45.9), 54695.19(3), 54810.9(5.2) 54928.6(2.3), 55213(2668), 55936.2(18.6), 57346(1.94), 57468.59(229), 58240.781(837.88)	1.16(19)	0.03	→ 0.16	2.99	3.09	1.28%

Note: glitch parameters for PSR J0537–6910 are gathered from Antonopoulou et al. (2018). Others are derived from our work and Jodrell Bank Glitch Catalogue.

Radhakrishnan, V., & Manchester, R. N. 1969, *Nature*, 222, 228
Ravenhall, D. G., & Pethick, C. J. 1994, *ApJ*, 424, 846
Ray, P. S., Guillot, S., Ho, W. C. G., et al. 2019, *ApJ*, 879, 130
Reichley, P. E., & Downs, G. S. 1969, *Nature*, 222, 229
Serim, M. M., Şahiner, Ş., éerri-Serim, D., Inam, S. ć., & Baykal, A. 2017, *MNRAS*, 471, 4982
Shabanova, T. V. 2009, *Astronomy Reports*, 53, 465
Shabanova, T. V. 2010, *ApJ*, 721, 251
Shaw, B., Lyne, A. G., Stappers, B. W., et al. 2018, *MNRAS*, 478, 3832
Sushch, I., Oya, I., Schwanke, U., Johnston, S., & Dalton, M. L. 2017, *A&A*, 605, A115
Urama, J. O., & Okeke, P. N. 1999, *MNRAS*, 310, 313
Wang, J., Wang, N., Tong, H., & Yuan, J. 2012, *Ap&SS*, 340,

307
Wang, N., Manchester, R. N., Pace, R. T., et al. 2000, *MNRAS*, 317, 843
Weisberg, J. M., Nice, D. J., & Taylor, J. H. 2010, *ApJ*, 722, 1030
Weltevrede, P., Johnston, S., Manchester, R. N., et al. 2010, *PASA*, 27, 64
Yu, M., Manchester, R. N., Hobbs, G., et al. 2013, *MNRAS*, 429, 688
Yuan, J. P., Wang, N., Manchester, R. N., & Liu, Z. Y. 2010, *MNRAS*, 404, 289
Zhou, S. Q., Zhou, A. A., Zhang, J., et al. 2019, *Ap&SS*, 364, 173
Zou, W. Z., Wang, N., Wang, H. X., et al. 2004, *MNRAS*, 354, 811